An investigation into alpha-particle properties and ranges, source-detector interaction and absorber thicknesses

Hiten Pragji
MSc Medical Physics (PGT)
9th December 2019

Abstract

This report investigated several properties of α particles emitted from a triple-α source containing the isotopes ^{239}Pu, ^{241}Am and ^{244}Cm. Absolute α-activities for ^{239}Pu, ^{241}Am and ^{244}Cm were calculated to be (1081.87 $\pm$ 32.9) s^{-1}, (1037.56 $\pm$ 32.2) s^{-1} and (65.75 $\pm$ 8.1) s^{-1}, respectively with experimental α-particle ranges of (3.66 $\pm$ 0.26) mg cm^{-2}, (4.25 $\pm$ 0.37) mg cm^{-2} and (4.94 $\pm$ 0.25) mg cm^{-2}, respectively. These values agree with theoretical predictions and confirm the presence of energy straggling at greater air pressures. Absorber thicknesses of polypropylene foil were calculated to be (6.6 $\pm$ 1.4) x 10^{-4} cm and (2.1 $\pm$ 0.1) x 10^{-3} cm for foil 1 and foil 2, respectively.

1 Introduction

Alpha-particle spectrometry (AS) is a widely used radiometric analysis technique that allows us to identify and determine, both quantitatively and qualitatively, α-emitting radionuclides. AS involves measuring emitted α-particle energies resulting from the radioactive decay of radionuclides and aims to quantify absolute activities, branching ratios in parent-daughter α-decay schemes, emission probabilities and relative half-lives. AS has many applications, for example, environmental radiation monitoring, health studies, radiation protection, nuclear technology, nuclear waste management and several research topics such as astrophysics and nuclear medicine. It is evident that this technique proves to be both useful and fascinating. Many instruments have been used for AS: gridded ionisation chambers, proportional counters, scintillation detectors and semiconductor detectors. We use a thermally diffused silicon (Si) PIN semiconductor detector which gives a very good energy resolution. Si diodes are near-ideal detectors of α-particles if operated at room temperature, for many reasons [1]. For instance, the amount of energy required to produce an electron-hole pair in typical semiconductor materials is considerably smaller than the energy needed to produce an ion pair in a gas detector. Additionally, the relatively high density of semiconductor detectors leads to more compact devices with quicker response times and high detection efficiencies. The main challenge in using Si detectors for AS is the limitation to the optimal energy resolution. Some of the typical uncertainties in AS are discussed in the IOP paper at [2]. The series of experiments detailed in this report aims to study the properties of α particles and their interaction with the Si PIN detector. First, we produce a calibrated energy spectrum of the triple-α source and determine the corresponding energy resolution and absolute activities. Secondly, after performing a more accurate calibration of the MCA, the relationships of peak energy and peak width with air pressure is explored. This is done by varying the air pressure around the source and detector. Using this data, we calculate the range of the α particles and compare them with values from theory. Lastly, the attenuation of α particles is studied by placing an absorber medium between the source and detector. Observing the resulting energy loss enables us to find the thickness of the medium.

2 Theory

2.1 Alpha decay

Alpha (α) decay is a radioactive decay process whereby a heavy nucleus ejects an α particle, that is a helium nucleus made up of two protons and two neutrons. α decay is the main process by which α particles are produced. The spontaneous emission of an α particle can be represented as

$$ {}^{A}_{Z}X_{N} \rightarrow {}^{A-4}_{Z-2}X'_{N-2} + \alpha, \tag{1} $$

where X is the decaying nucleus and X' is the daughter nucleus. The typical energy released is about 5 MeV and about 98% of this energy is carried by the α particle, with the remaining 2% carried by the much heavier fragment X'. Understanding the decay process fully requires a study of the conservation of energy, linear momentum and angular momentum. One of the most important features of α decay is that α emitters with large disintegration energies have short half-lives and conversely. This is called the Geiger-Nuttall law, written as

$$\log_{10} \lambda = -a_1 \frac{Z}{\sqrt{E}} + a_2, \tag{2}$$

where λ is the decay constant, Z is the atomic number, E is the total kinetic energy of X and X', and a_1 and a_2 are constants. Equation (2) shows that the half-life of the radioactive isotope is exponentially dependent on decay energy and that large variations in half-life correspond to relatively small changes in decay energy. The reader may find the Wolfram demonstration in [3] to be a useful visual aid. Equation (2) can be derived using a quantum-mechanical theory that we will now briefly touch upon.

2.1.1 Semi-classical theory of alpha decay

Consider an α particle trapped inside a heavy nucleus by the Coloumb barrier. Through a process of quantum-mechanical barrier penetration, also known as tunnelling, the α particle is able to escape to the outside world. This process is illustrated in Figure 1, where the potential energy between the α particle and daughter nucleus, $V(r)$, is plotted against the distance between their centres, r. The

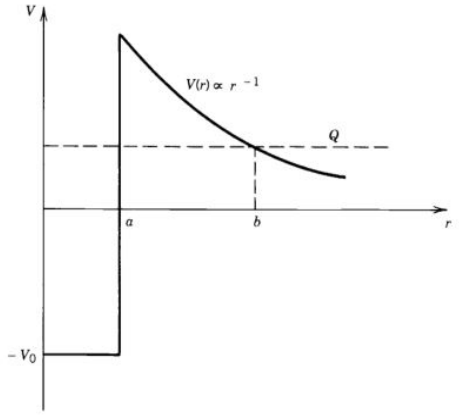

Figure 1: Schematic for the potential energy of an α particle for the daughter-nucleus system. [4]

dotted line in Figure 1 represents the decay Q-value, which must be positive otherwise the α particle is bound and cannot escape. Inside the nucleus ($r < a$), the particle is confined (its movement is restricted to this region only) to a finite square well with potential $-V_0$, where $V_0 > 0$. Within the barrier region $a < r < b$, $V(r)$ is a decreasing function of r. This barrier region can be thought of as a set of narrow rectangular barriers of width dr, which the α particle must penetrate in order to escape the nucleus. The remainder of this theory involves calculating the probability that the α particle exists as a recognisable entity inside the nucleus before its emission. A thorough description is found in [4].

2.2 Alpha radiation detection

Between the years 1908 and 1913, Geiger and Marsden conducted a series of gold foil experiments in which a narrow beam of α particles were passed through very thin gold foil and collected by a zinc sulfide screen. The findings led to the discovery of the atomic nucleus. Experiments such as these were the earliest methods of α-particle detection, followed by detection by ionisation chambers, proportional counters and Geiger-Müller tubes. Each have their advantages and disadvantages, however today semiconductor detectors are employed for their good energy resolution and detection efficiency. In this experiment, we use a photodiode made of silicon (Si), a semiconducting material. The photodiode

converts incident photons to an electrical current. It is characterised as a PIN diode consisting of a p-type and n-type semiconductor region, between which an intrinsic layer, also known as the bulk region, is placed. Further details on the physics and electronics of PIN diodes is found at [5]. If we assume that the detector has 100% efficiency, that is every α-particle reaching the detector will interact within it and be counted, we can calculate the absolute α-activity I [6]:

$$I = \frac{C_\alpha}{f} \times \frac{4\pi d^2}{A}, \tag{3}$$

where C_α is the counting rate in s^{-1}, f is the fractional intensity of the α-particle energy peak, d is the source-detector distance and A is the area of the detector surface.

2.3 Stopping power and the Bethe-Bloch formula

The linear stopping power S for charged particles in an absorber material is defined as the differential energy loss for that particle within the material divided by the corresponding differential path length:

$$S = -\frac{dE}{dx}. \tag{4}$$

It is useful to define a specific energy loss along a particle track for a nonrelativistic particle. This is given by the Bethe-Bloch formula:

$$-\frac{dE}{dx} = \frac{4\pi e^4 z^2}{m_0 v^2} \rho_e \ln\left(\frac{2m_0 v^2}{I}\right), \tag{5}$$

where ze is the ion charge, m_0 is the electron rest mass, v is the ion velocity, ρ_e is the electron density of the absorber and I is the mean excitation and ionisation potential of the absorber. Eq (5) therefore shows that for a given nonrelativistic particle, dE/dx varies as $1/v^2$. Of importance also is the fact that materials with high Z numbers result in the greatest linear stopping power.

2.4 Energy loss in thin absorbers

When an alpha particle passes through a thin absorber of thickness Δx, the material on average has a stopping power for α particles attenuated by it, due to interactions with absorber atoms. The stopping power of the foil varies with the energy of the particles interacting in the foil. Thus, the stopping power of the material before interaction, $(dE/dx)_{E_0}$, corresponds to the incident α-particle energy E_0. The same is said for E_f, the exit energy of the α particle. Assuming that (dE/dx) varies linearly across the thin absorber, we can calculate the average stopping power [7]:

$$\left(\frac{dE}{dx}\right)_{average} = \frac{(dE/dx)_{E_0} + (dE/dx)_{E_f}}{2} \tag{6}$$

Using Equation (6), we can find the energy loss ΔE through the medium [7]:

$$\Delta E = \left(\frac{dE}{dx}\right)_{average} \Delta x. \tag{7}$$

2.5 Energy resolution

The energy resolution is defined by a Gaussian distribution about the average pulse height and is proportional to the full width at half maximum (FWHM) of the Gaussian. Thus, knowing the height of the peak centroid and the FWHM will allow us to estimate the energy resolution of the detector. Any sources of fluctuations in the signal from the detector will add in quadrature to give the total energy resolution $FWHM_{tot}$ of the system:

$$FWHM_{tot}^2 = FWHM_{stat}^2 + FWHM_{elec}^2, \tag{8}$$

where $FWHM_{stat}$ is the peak width due to counting statistics only, and $FWHM_{elec}$ is the width of a pulser peak generated by the injection of charge into the preamplifier (discussed in Section 3.3.2) [6]. It is important to note that the smaller the value for the energy resolution, the better the detector will be able to distinguish between two radiations whose energy peaks are close together.

2.6 Energy straggling

The total energy loss through the absorber, in a segment of the particle track, is represented by a stochastic quantity. This quantity has an asymmetric distribution around the average energy loss and is described in terms of a straggling function and varies across the ion's range [8]. The reason for this is that the number of collisions required to bring the ion to rest and the energy lost per collision within the medium will vary slightly between particles. Additional changes such as altering gas pressure in the chamber surrounding the source can skew the energy distribution further, leading to widened energy peaks in the spectra. This is called energy straggling and may be described by

$$FWHM = 4.16(\Delta x)^{1/2} \tag{9}$$

where the FWHM is in keV and Δx is the air-path thickness in mg cm^{-2}[6].

2.7 Particle range

Range is defined as the distance traveled by the ion from the source to the point where it loses all of its energy. It is possible to integrate Equation (5) over the full ion path to obtain an expression for its range in the material, however the expression collapses at low values of the α-particle velocity. Instead, we follow an empirical relation given by

$$R_\alpha = 0.318 E_\alpha^{3/2} \text{ cm of air}, \tag{10}$$

where E_α is in MeV, air is at standard pressure and temperature (STP) [6] and R_α has units of mg cm^{-2}. It is also possible to determine the range experimentally. From the ideal gas law, we have

$$\rho = \frac{P}{RT}, \tag{11}$$

where P is the gas pressure in pascals, R is the molar gas constant and T is the temperature in kelvin. Here, the pressure is analogous to a 'thickness' at which the α particle has finally stopped in the absorber. Finally, Equation (9) is used to find the range of the α particle [9]:

$$R_\alpha = \rho \times d. \tag{12}$$

3 Experimental method

3.1 Apparatus

1. **ORTEC Model 676 Alpha-King spectrometer NIM**: nuclear instrumentation module (NIM) containing a small vacuum chamber in which the α source is placed. There are three dials and one switch on the module. One dial is for controlling the energy range, the second is for adjusting the injected pulser and the third is to change the vacuum pump setting between pump, hold and vent. The remaining switch is to select between bias and pulser. This NIM contains a built-in preamplifier and shaping amplifier.
2. **Hamamatsu Si PIN photodiode S1223-01**: the semiconductor detector that is used to detect the emitted radiations. Specifications can be found at [10].
3. **ORTEC 4006 Minibin and Power Supply**: accommodates up to six NIM-standard modules and has two standard preamplifier power outlets.
4. **Balston Vacuum Chamber Type 9956-12**: the chamber is an enclosed vessel from which air is removed by use of a vacuum pump. It is attached to the vacuum pump. Evacuation of the pump plays an important role for the investigation into α particle range in air.
5. **Edwards High Vacuum Pump E2M-1.5**: creates a partial vacuum around the source and detector in the NIM. The attached pressure gauge measures the pressure (in millibar) in the chamber.

6. **ORTEC EASY-MCA-8K (Multi-Channel Analyser)**: uses a fast analogue-to-digital converter (ADC) to record an input signal consisting of pulses. It stores pulse data either via pulse-height analysis (PHA) or multichannel scaling mode (MCS). We require PHA mode because this gives us a pulse-height spectrum that we can use to analyse the energy peaks. Connection to PC is via the USB2 cable.

7. (a) **S263.PH triple-alpha source set**: total initial activity of 5 kBq. The α-emitters are ^{239}Pu, ^{241}Am and ^{244}Cm, (b) **single ^{241}Am source**.

8. **ORTEC MAESTRO MCA PC software**: controls the MCA and is used to interpret the acquired data from the MCA.

9. **2x polypropylene foils** of unknown thickness.

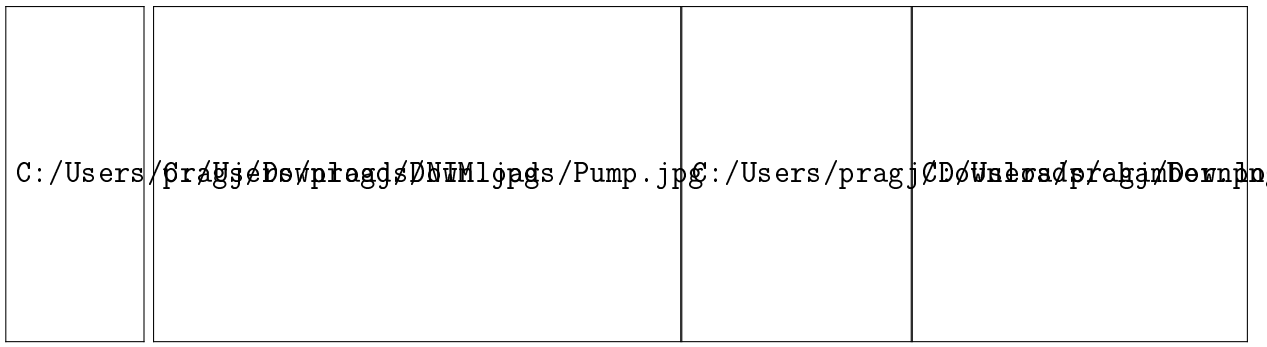

Figure 2: From left to right: NIM, vacuum pump, vacuum chamber [11], Si PIN diode [10].

3.2 Schematics

Figure 3: Schematics of the experimental setup.

3.3 Procedure

3.3.1 Experiment 1

Using tweezers, the triple-α source was placed inside the NIM at $d = 1.5 \pm 0.1$ cm from the detector. The energy range was set to 3 - 8 MeV and the toggle switch of the NIM was set to 'BIAS'. Creation of a vacuum within the chamber followed a step-by-step procedure outlined in the laboratory script at [6]. We ran an acquisition for 300 s, giving a spectrum of counts versus channel number that was then calibrated using the MCA and the peak energies of each isotope: 5155 keV for ^{239}Pu, 5486 keV for ^{241}Am and 5805 keV for ^{244}Cm. This data was used to determine the corresponding FWHM and count rate for each peak, and subsequently the absolute α-activity of each isotope using Equation (4).

3.3.2 Experiment 2

Toggling the switch on the NIM to 'PULSER' allowed for more accurate calibration of the MCA by injecting a small charge into the preamplifier. The pulser gain was adjusted to appear close to the ^{241}Am peak and Equation (8) was used to calculate $FWHM_{stat}$. We recorded spectra at six different values of air pressure and looked at the relationship of air pressure with peak energy and peak width (FWHM). The air pressure in the chamber was altered by following a step-by-step process outlined in [6]. Extrapolating the curves on the graphs to zero energy allowed for the calculation of α-particle ranges for each isotope at different pressures, which were then compared with theoretical values obtained by using Equation (10). The relationship given in Equation (9) was explored. Due to time constraints, it was not possible to look at the relationship between peak intensity and pressure.

3.3.3 Experiment 3

Using the single ^{241}Am source and without altering the pressure in the chamber, we measured the energy of the α particles as they passed through each polypropylene foil. Comparisons with the spectrum taken without an additional absorber medium allowed us to calculate the layer thickness of each foil, using the stopping power and range tables provided at [12].

4 Results

4.1 Experiment 1

A logarithmic spectrum of counts versus energy was plotted and shown in Figure 4. Three main peaks are identified and labelled accordingly. Using a logarithmic y-scale allows us to view weak fine structure peaks which originate from α-transitions to quantum states of the daughter nuclei, ^{235}U, ^{237}Np and ^{240}Pu, respectively. The count rates in each of the main peaks was found by using the

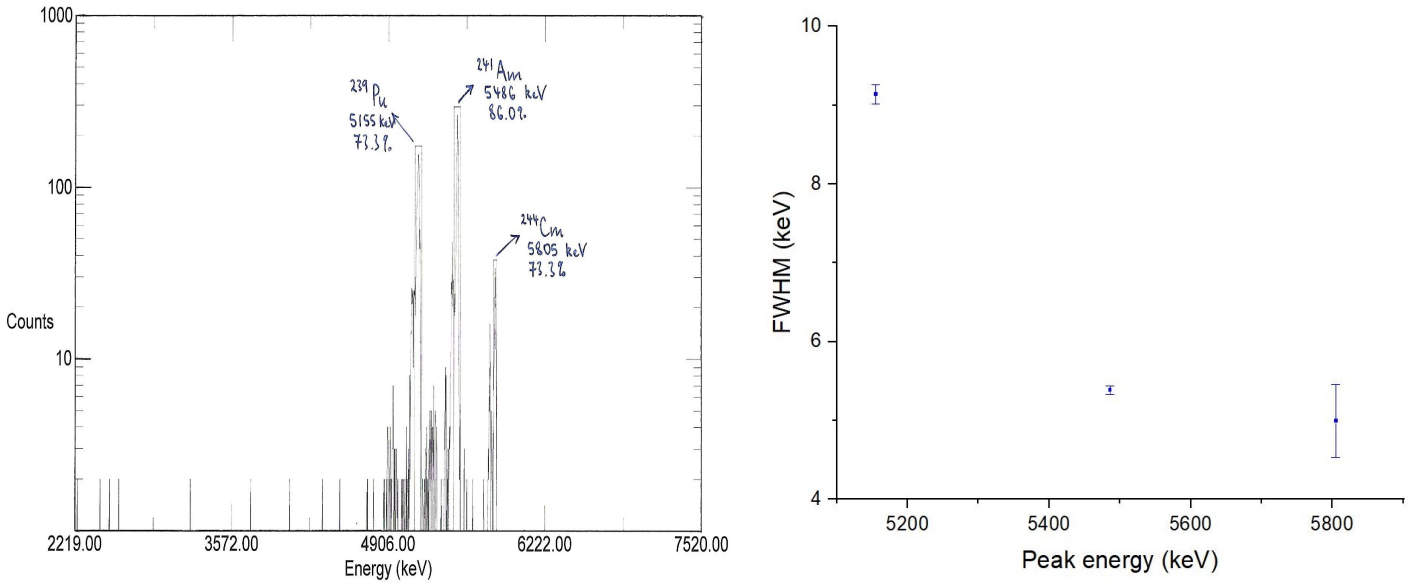

Figure 4: Left: calibrated energy spectrum for the triple-α source. Right: corresponding FWHM of the energy peaks as a function of peak energy.

region of interest (ROI) features in MAESTRO and it was found, using Equation (4), that the absolute α-activities decreased as the isotope mass number increased. These values are shown in Table 1.

4.2 Experiment 2

Using the ROI features, values of 11.67 keV and 4.43 keV were found for $FWHM_{tot}$ and $FWHM_{elec}$, respectively. Using Equation (8), this gives a value of $FWHM_{stat}$ equal to 10.8 keV. Assessing the MCA's response was successful and its linearity was confirmed by inserted a pulser peak at 5.49 MeV

Isotope	Peak energy (keV)	BR (%)	Count rate (s^{-1})	I (s^{-1})
^{239}Pu	5155	73.3	3.62	1081.87 ± 32.9
^{241}Am	5486	86.0	4.09	1037.56 ± 32.2
^{244}Cm	5805	73.3	0.22	65.75 ± 8.1

Table 1: Tabulated values of the absolute α-activity of each isotope in the triple-alpha source.

- close to the ^{241}Am peak - and performing a calibration at lower peak energies (see Figure 5). Table 2 thus shows that halving the pulser output subsequently halves the peak energy.

Pulser output (MeV)	Peak energy (keV)
0.69	685.75
1.38	1371.5
2.75	2743
5.49	5486

Table 2: Tabulated results showing the linearity of the response from the MCA.

The variation of peak energy with air pressure for the triple-α source is shown in Table 3 and plotted in Figure 6. It is apparent that peak energy decreases as air pressure increases.

Air pressure (mbar)	Peak energy (keV)			FWHM (keV)		
	^{239}Pu	^{241}Am	^{244}Cm	^{239}Pu	^{241}Am	^{244}Cm
30	5155	5486	5805	9.61	6.13	6.53
200	4533.9	5108.8	5633.6	22.2	20.2	22.2
400	4028.4	4635.6	5115.4	35.9	35.1	30.0
600	3511.4	4128.7	4707.5	52.3	47.8	37.1
800	2893.8	3580.8	4128.7	72.3	64.2	58.5
1000	2546.7	3048.3	3607.8	93.7	79.9	72.0

Table 3: Tabulated peak energies and peak widths for each isotope at different air pressures.

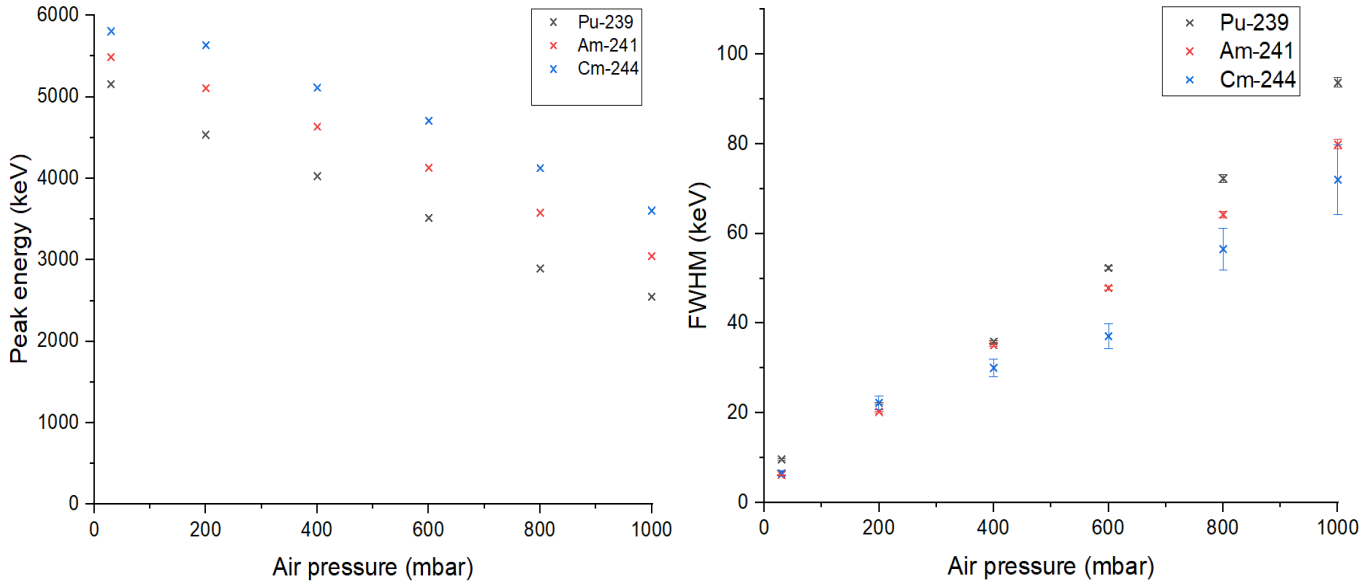

Figure 5: Left: Variation of each isotope's peak energy with air pressure. Right: Change in FWHM of the peaks as air pressure is increased. In both cases, the fit is clearly linear.

Table 4 compares the theoretical values of α-particle ranges obtained using Equation (7) with experimental values obtained by extrapolating the best fit line for the data in Figure 5 to the point at which the peak energy is zero. This was done in Microsoft Excel, by first plotting the graph as is shown, then

adding a trendline with a fitting equation. Thus the value of air pressure at zero peak energy is easily calculated by using Equations (9) and (10).

Isotope	Energy (MeV)	Range (mg cm^{-2})	
		Theoretical	Experimental
Pu-239	5.155	3.72	3.66 ± 0.26
Am-241	5.486	4.09	4.25 ± 0.37
Cm-241	5.805	4.45	4.94 ± 0.25

Table 4: Comparison of theoretical and experimental alpha-particle ranges for three radioisotopes.

The variation of energy resolution with α-particle range is shown in Figure 6. The graph shows that an increase in the air-path thickness consequently leads to an increase in the FWHM. This confirms the existence of energy straggling as predicted by Equation (9).

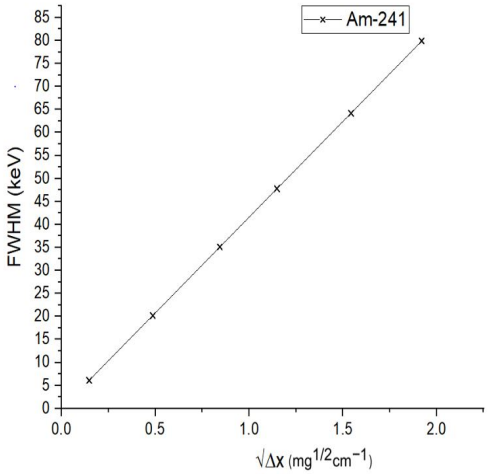

Figure 6: Variation of the Am-241 FWHM with the square root of the air thickness.

4.3 Experiment 3

A spectrum for the single ^{241}Am source was obtained and shown in Figure 7. Using the ROI feature, its peak energy was found to be 5570.43 keV. Two further spectra were acquired, shown in Figures 8 and 9, this time using two polypropylene foils of different thickness. The peak energies for these spectra were 5032.72 keV and 3617.22 keV, respectively, giving energy shifts of $\Delta E_1 = 537.71$ keV for foil 1 and $\Delta E_2 = 1953.21$ keV for foil 2. Using the tables at [12], Equations (6) and (7), it was found that the thickness of foil 1 was (6.6 ± 1.4) x 10^{-4} cm and for foil 2 it was (2.1 ± 0.1) x 10^{-3} cm.

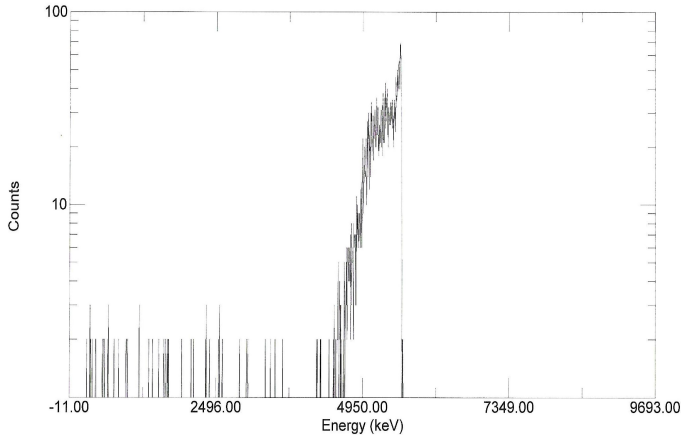

Figure 7: ^{241}Am energy spectrum without the use of foil.

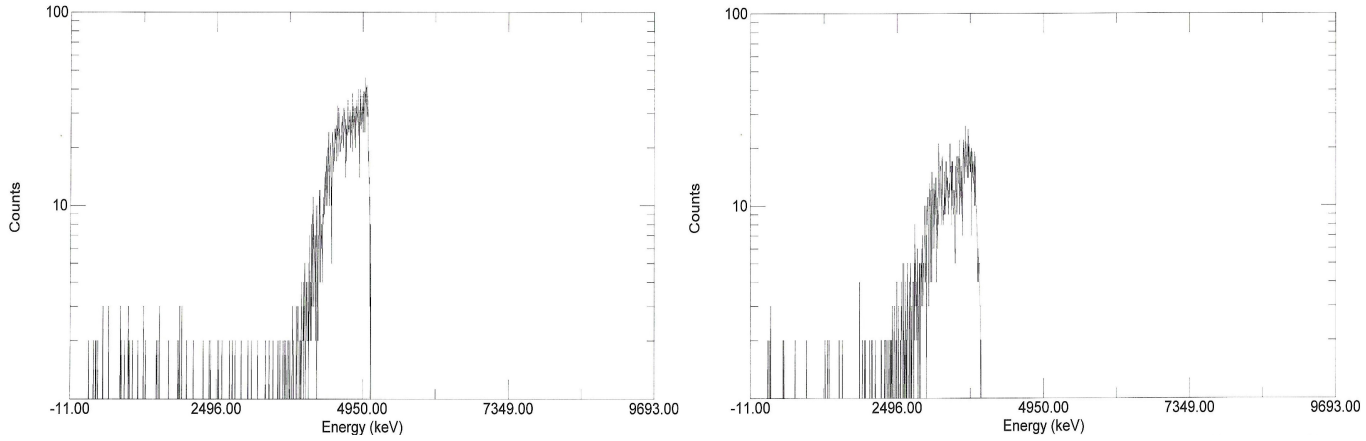

Figure 8: ^{241}Am energy spectrum for foil 1 (left) and foil 2 (right).

5 Discussion of results and errors

The absolute α-activities found in Experiment 1 agree with the predictions set forth by Equation (3); as the ratio of count rate to fractional intensity decreases, so does the activity. However, we have also made the assumption that the detector has 100% efficiency. There is also an error on the count rate. This behaviour may be verified using the Geiger-Nuttall law, but this would be inaccurate due to the time elapsed since the sample was created. The corresponding FWHM of each peak in Figure 4 is shown to decrease with increasing peak energy, which means that the energy resolution improves at greater peak energies, but it is important to note that the error on the FWHM for ^{244}Cm is considerably large in comparison to the other two errors. In Experiment 2, it was found that $FWHM_{stat}$ contributes to the majority of the overall FWHM in the presence of a pulser peak, and that $FWHM_{elec}$ is relatively small. The effect that halving the pulser output has on the peak energy shows that the MCA can be calibrated at lower energies too. The process of varying the air pressure in the NIM chamber was affected by parallax whilst measuring the value on the pressure gauge. This could be avoided by using an electronic reader instead. Both of the graphs in Figure 5 successfully represent the effect that air pressure has in the measurement of α-particle energies; the greater the pressure, the more likely it is for collisions to occur and therefore more energy is lost across the range of the particle. As the air pressure increases, the energy resolution also decreases due to energy straggling. Even though straggling is not deterministic in nature, our graphs show that the relationship is clearly linear, as expected. The experimental values of range in Table 4 agree very well with theory. This confirms that the air thickness required to fully stop an α particle increases with the isotope's peak energy. Though, the fitting equation used to determine this value is not the most precise method because it is essentially a form of forecasting; in fact, a significant improvement would have been to have access to a vacuum pump able to produce pressures greater than 1000 mbar. Another discrepancy to account for is the use of Equation (11) despite the fact that air is not an ideal gas. In Experiment 3, it was found that the thickness of both foils are different and this is predictable by looking at the energy shifts between Figures 7 and 8. The variation of energy loss with absorber thickness is thus verified both experimentally and theoretically (using Equation (7)). Uncertainties in the foil thickness could arise from the fact that we have assumed a linear variation of stopping power through the foil; realistically this may require correction. Also, any rapid venting of the chamber could damage the foil. Other sources of error include background radiations, human error in the selection of ROIs in MAESTRO, uneven placement of the source under the detector and any prior damage to the detector.

6 Conclusion

In this investigation, we have successfully used AS to determine various quantities and relationships typical of α emitters. The absolute α-activities of ^{239}Pu, ^{241}Am and ^{244}Cm were calculated to be 1081.87 $\pm$ 32.9 s^{-1}, 1037.56 $\pm$ 32.2 s^{-1} and 65.75 $\pm$ 8.1 s^{-1}, respectively and ranges were found to be 3.66 $\pm$ 0.26 mg cm^{-2}, 4.25 $\pm$ 0.37 mg cm^{-2} and 4.94 $\pm$ 0.25 mg cm^{-2}, respectively. Experimental ranges

compared favourably with theoretical predictions. Energy straggling was observed clearly and a linear relationship was found to exist between air thickness and peak width. Using polypropylene foils as absorber media between the source and detector, it was possible to find the thickness of foil 1 and foil 2, having values of 6.6 x 10^{-4} cm and 2.1 x 10^{-3} cm, respectively. By eliminating as far as possible any potential sources of error, it can be shown that AS is a very reliable radiometric analysis technique and that our Si PIN detector does indeed perform well at room temperature.

Acknowledgements

I would like to thank the laboratory demonstrators for their support in helping me to understand the experimental techniques involved in this investigation. I also thank my laboratory partner, Ramin Fard, for his continued assistance with all things experimental.

Appendices

The parameter R absolutely defines the energy resolution of the detector by the equation

$$R = \frac{FWHM}{H_0}, \tag{13}$$

where H_0 is the height of the peak centroid in the Gaussian distribution described in Section 2.5. Since the response of most detectors is roughly linear, the average pulse amplitude $H_0 = KN$, where K is a proportionality constant and N is the total number of charge carriers. [1]

References

[1] G. F. Knoll, *Radiation detection and measurement.* John Wiley & Sons, 2010.

[2] S. Pommé, "Typical uncertainties in alpha-particle spectrometry," *Metrologia*, vol. 52, no. 3, p. S146, 2015.

[3] S. M. Blinder. Gamow model for alpha decay: The geiger-nuttall law. https://demonstrations.wolfram.com/GamowModelForAlphaDecayTheGeigerNuttallLaw/#embed.

[4] Krane, *Introductory Nuclear Physics*, 2nd ed. Wiley, 1988.

[5] L. Simms. Chapter 2, overview of silicon pin detectors. https://lancesimms.com/Thesis/ThesisChapters/Chapter2.pdf.

[6] U. of Surrey. Rad7 - alpha-particle spectroscopy. https://surreylearn.surrey.ac.uk/d2l/le/content/191583/viewContent/1632366/View.

[7] U. of Sheffield. N2: Alpha particle attenuation in matter measurements using a semiconductor detector. https://www.sheffield.ac.uk/polopoly_fs/1.14264!/file/N2.pdf.

[8] M. Berger, M. Inokuti, H. Andersen, H. Bichsel, D. Powers, S. Seltzer, D. Thwaites, and D. Watt, "6. energy-loss straggling," *Reports of the International Commission on Radiation Units and Measurements*, no. 2, pp. 61–68, 1993.

[9] I. Etim, E. William, and S. Ekwe, "Alpha-particle spectroscopy and ranges in air."

[10] H. Photonics. Si pin photodiode s1223-01. https://www.hamamatsu.com/us/en/product/type/S1223-01/index.html.

[11] Balston. Balston vacuum pump inlet exhaust filters. http://www.balstonfilters.com/_literature_176312/Vacuum_Pump_Filters.

[12] NIST. Astar: Stopping power and range tables for alpha particles. https://physics.nist.gov/cgi-bin/Star/ap_table.pl.